

Spurious Crests in Second-Order Waves

M. A. Tayfun

Abstract—Occurrences of spurious crests on the troughs of large, relatively steep second-order Stokes waves are anomalous and not an inherent characteristic of real waves. Here, the effects of such occurrences on the statistics described by the standard second-order stochastic model are examined theoretically and by way of simulations. Theoretical results and simulations indicate that when spurious occurrences are sufficiently large, the standard model leads to physically unrealistic surface features and inaccuracies in the statistics of various surface features, in particular, the troughs and thus zero-crossing heights of large waves. Whereas inaccuracies can be fairly noticeable for long-crested waves in both deep and shallower depths, they tend to become relatively insignificant in directional waves.

Keywords—Large waves, non-linear effects, simulation, spectra, spurious crests, Stokes waves, wave breaking, wave statistics.

I. INTRODUCTION

THE second-order Stokes model describing long-crested surface waves is of the form [1]

$$\eta = \eta_1 + \eta_2 = a \cos \chi + \frac{1}{2} a^2 k f \cos 2\chi, \quad (1)$$

where a = wave amplitude, k = wave number, $q = kd$, d = mean water depth, χ = wave phase, ω = angular frequency, ak = wave steepness, and

$$f = [\cosh q (2 + \cosh 2q)] / 2 \sinh^3 q \quad (2)$$

is a dimensionless measure of the effect of relative water depth q on the second-order correction η_2 . In general, $f \geq 1$, $f \rightarrow 1$ in deep water where $q > \pi$, and $f \rightarrow 3/2q^3$ in shallow water where $q < \pi/10$, approximately

The relative validity and convergence of the preceding deterministic model regarded as the first two terms of a power series expansion in wave steepness ak are often inferred from the ratio test [1]. The latter imposes an upper limit to the steepness of waves that can be described by (1) and higher-order Stokes models in shallow water. However, unless

$$ak \leq 1/2f, \quad (3)$$

(1) describes anomalous wave forms characterized with spurious crests at wave troughs. It turns out that (3) is a more stringent condition than the ratio test [1]. Secondary crests do not appear in third- and higher-order Stokes waves.

The steepness of large waves also tends to be limited by an

M. A. Tayfun, is with Kuwait University, Kuwait (phone: 965-6622-7814; fax: 965-2481-7524; e-mail: aziztayfun@usa.net).

upper bound often related to wave breaking. An approximation for such a bound is given by [2]

$$ak \leq 0.448 \tanh q. \quad (4)$$

This expression tends to $ak \leq 0.448q$ in shallow waters and to $ak \leq 0.448$ in deep water where the upper bound $ak = 0.448$ is better known as the Stokes limit. The upper limit described by (4) is an approximate extension of the same concept to finite water depths. Comparisons of (4) to laboratory and oceanic data suggest that it is not a consistent indicator of wave breaking or its inception [3]. However, it does indicate an upper bound to the heights of large waves, breaking or otherwise [3]-[5]. One refinement recently proposed replaces 0.448 with 0.55 in deep water [6].

Fig. 1 illustrates (2) and the upper limits of (3) and (4). It is seen that constraint (3) on spurious crests for $q \leq 2$ in shallow and transitional water depths, and (4) for $q > 2$ in transitional and deep waters indicate if (1) depicts physically valid approximations to large waves free of spurious crests. Evidently, if 0.448 in (4) were to be replaced with 0.55, then (3) would be the only principal constraint on the physical validity of (1).

To illustrate wave forms described by (1), assume that $q = 0.4\pi$ and consider waves represented by three discrete points in Fig. 1 and characterized by $ak = 0.01, 0.2$, and 0.4 , respectively. Fig. 2 displays the explicit wave profiles predicted from (1). The first case where $ak = 0.01$ is well below the upper limits of (3)-(4) represents a linear wave, effectively. The remaining two cases display the same wave profile modified by the second-order corrections as wave steepness increases. Case $ak = 0.2$ is near but below the upper bound of (3) whereas $ak = 0.4$ violates (3) and (4) both. In the profiles for $ak = 0.01$ and 0.2 , wave troughs appear concave upward and represent physically acceptable approximations within the range of validity of (1). In contrast, case $ak = 0.4$ is physically unrealistic, displaying an anomalous trough section characterized by a negative spurious hump or crest at $\chi = \pi$ and two identical troughs symmetrically located on both sides of and below the spurious crest at $\chi_1 = \pi - \cos^{-1}(1/2akf)$ and $\chi_2 = \pi + \cos^{-1}(1/2akf)$, respectively. Such wave forms lie outside the realistic range of (1).

Now, note that in all three cases considered, $\eta/a = 1 + (1/2)akf$ at $\chi = 0$ and 2π where wave crests appear, irrespective of (3). So long as (3) holds, $\eta/a = -1 + (1/2)akf$ at $\chi = \pi$ where a regular wave trough is seen, as in cases where $ak = 0.01$ and 0.2 . Evidently, the second-order correction is $(1/2)akf$. It displaces crests and troughs both upward equally. Thus, the wave height, H , defined as the elevation difference between the maximum and minimum of a zero up- or down-

crossing cycle is $2a$, the same as in the linear profile. However, if (3) is violated as in case $ak = 0.4$, a negative

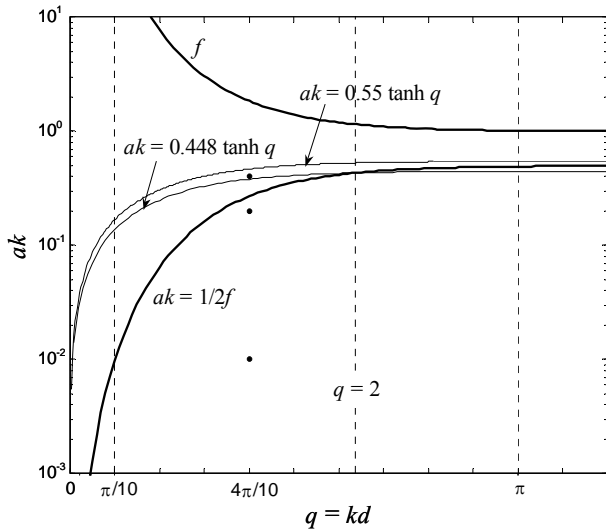


Fig. 1 Upper bounds (3)-(4) on wave steepness

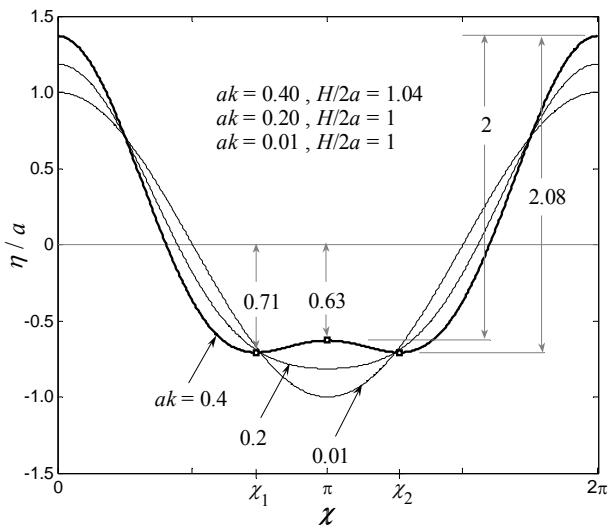


Fig. 2 Second-order waves for $ak = 0.01, 0.2$, and 0.4 at $q = 0.4\pi$

spurious crest will appear at $\chi = \pi$ where

$$\frac{\eta}{a} = -1 + \frac{1}{2}akf, \quad (5)$$

as before, but also two anomalous wave troughs at $\chi = \chi_1$ and χ_2 where

$$\frac{\eta}{a} = -\frac{1}{2}akf - \frac{1}{4akf}. \quad (6)$$

Since $2akf > 1$, (6) is larger than (5) in absolute value. For

case $ak = 0.4$ of Fig. 2, $2akf = 1.483$. As a result, $\eta/a = -0.63$ and $\eta/a = -0.71$ from (5) and (6), respectively. In other words, the trough described by (6) is about 13% deeper than (5). So, an immediate consequence of spurious occurrences is that trough amplitudes would appear larger than they should within the physically valid range of the second-order theory. This also leads to $H = 2.08a$ for $ak = 0.4$ with an overestimation error of about 4% relative to $2a$. Thus, $H/2a = 1$ only if $ak \leq 1/2f$. Otherwise

$$\frac{H}{2a} = \frac{1}{2} \left(1 + akf + \frac{1}{4akf} \right) > 1. \quad (7)$$

Spurious crests and anomalous double troughs are not systemic features observed in oceanic waves or in mechanically generated waves. Also, whereas the effects of constraints (3)-(4) on the deterministic second-order Stokes theory are straightforward to predict, it is hardly the case for the standard second-order random model used for describing oceanic waves [7]-[10]. The latter generalizes (1), taking into account the random nature of the wind-disturbed sea surface characterized by directional spectrum. It has a two-term form, the same as (1), but second-order correction η_2 and so η are algebraically a good more cumbersome and not amenable to analytical manipulations with ease. And, η is not immune against errors due to occurrences of spurious crests. As previously mentioned, such errors do not arise in third- and higher-order Stokes expansions, but there is no explicit stochastic model for describing third- or higher-order random waves similar to the standard second-order model.

Over the years, the standard model and/or simulations derived from it have been used in developing a variety of theoretical results of practical value on the nature and statistics of a variety of surface features observed in oceanic measurements. Some of these are approximations based on the Gram-Charlier series expansions of distributions describing surface elevations, slopes, wave envelopes, and phases [4], [8], [11]. Others such as the distributions describing the statistics of wave heights, crests, troughs and wave groups are either narrowband approximations [12]-[14], or they represent asymptotic limits valid for large waves [15]-[22], [26]. All these appear to work reasonably well in describing oceanic waves characterized by simple wind-wave spectra.

The standard model is also used in simulations for validating a theoretical result [20]-[22], [25] or as an exploratory tool for investigating the statistical nature of wave characteristics not amenable to theoretical analyses [10]. If certain spectral and statistical parameters in such simulations are specified arbitrarily or in a manner mimicking those observed in a severe sea state, then the resulting statistics describing various surface features can be affected by errors arising from possible occurrences of spurious crests and anomalous double troughs. Simulated wave heights can also violate upper bounds described by breaking criteria such as (3), leading to unrealistic results or flawed conclusions. Such errors are more likely to appear in large waves of interest, both

theoretical and practical. The present study explores such errors and their effects on various statistics of large waves based on the asymptotic theories [16]-[24].

II. SECOND-ORDER RANDOM MODEL

A. Model and Definitions

The second-order random representation is of the form $\eta = \eta_1 + \eta_2$. At a fixed point, say $(x, y) = (0, 0)$ for simplicity, η_1 is described in time t by

$$\eta_1 = \int \cos[\omega t + \varepsilon(\mathbf{k})] dZ(\mathbf{k}), \quad (8)$$

where \mathbf{k} denotes wave-number vector with direction θ and modulus k such that $\omega^2 = gk \tanh q$, ε 's are independent random phases uniformly distributed in $(0, 2\pi)$, and

$$dZ(\mathbf{k}) = [2E(\mathbf{k}) d\mathbf{k}]^{1/2}. \quad (9)$$

Here, E is the directional wave-number spectrum (density). Directional spectrum F defined over the frequency-direction domain follows from $E d\mathbf{k} = F(\omega, \theta) d\omega d\theta$.

Ordinary spectral moments are:

$$m_j = \iint \omega^j F(\omega, \theta) d\omega d\theta = \int \omega^j S(\omega) d\omega, \quad (10)$$

where S represents the frequency spectrum. The variance is $\sigma^2 = m_0$, $\omega_m = m_1/m_0$ = spectral-mean frequency, and

$$v = [(m_0 m_2 / m_1^2) - 1]^{1/2} \quad (11)$$

serves as a measure of bandwidth for S . An integral measure of wave steepness is $\varepsilon_p = \sigma k_p$, with k_p = spectral-peak wave number. Finally, the upper (+) and lower (-) envelopes of η_1 are defined by

$$\pm \xi = \pm(\eta_1^2 + \hat{\eta}_1^2)^{1/2}, \quad (12)$$

where $\hat{\eta}_1$ denotes the Hilbert transform of η_1 . Assuming that $\omega > 0$, $\hat{\eta}_1$ follows from (8) by replacing cosine term with sine.

The second-order correction can be expressed as

$$\eta_2 = \eta_2^+ + \eta_2^-, \quad (13)$$

where

$$\eta_2^\pm = \frac{1}{4} \iint K^\pm \cos \Omega^\pm dZ(\mathbf{k}) dZ(\mathbf{k}'), \quad (14)$$

$$\Omega^\pm = (\omega \pm \omega')t + \varepsilon(\mathbf{k}) \pm \varepsilon(\mathbf{k}'), \quad (15)$$

and K^\pm are second-order kernels associated with the frequency sum and difference terms in (13). The explicit forms of the

latter are rather lengthy and cumbersome. They are given elsewhere [7]-[10] and not repeated here for economy of space.

In the most general case, the statistical structure of η and the range of its relative validity are not adequately understood, especially, in transitional water depths. In the so-called weakly nonlinear theory, η_1 provides the bulk of the surface description. It is zero-mean Gaussian with variance $\sigma^2 = m_0$. Second-order correction η_2 is orthogonal to η_1 , zero-mean but non-Gaussian with variance

$$\langle \eta_2^2 \rangle = \iint G(\mathbf{k}, \mathbf{k}') E(\mathbf{k}) E(\mathbf{k}') d\mathbf{k} d\mathbf{k}', \quad (16)$$

where $G = (K^{+2} + K^{-2})/4$. As in the deterministic theory, η_2 imposes a well-known vertical skewness on η_1 [7]-[11]. This is described by the skewness coefficient $\lambda_3 = \langle \eta^3 \rangle / \sigma^3$, given by

$$\lambda_3 = \iint K(\mathbf{k}, \mathbf{k}') E(\mathbf{k}) E(\mathbf{k}') d\mathbf{k} d\mathbf{k}' / m_0^{3/2}, \quad (17)$$

where $K = 3(K^+ + K^-)/2$.

B. Theoretical Distributions

There are several theoretical distributions describing various surface features implied by the standard model. In order to elaborate some of these distributions, assume that all elevations are scaled with $\sigma = m_0^{1/2}$. On this basis, an approximation for the probability density of scaled η follows from the narrowband model [12] in the form [27]

$$p_\eta = \exp[-(Z-1)^2 / 2\mu^2] / Z\sqrt{2\pi} ; \quad \eta > -1/2\mu, \quad (18)$$

$$\approx 0 ; \quad \eta \leq -1/2\mu,$$

where $Z = (1+2\mu\eta)^{1/2}$ and $\mu \approx \lambda_3 / 3$. As $\lambda_3 \rightarrow 0$, the preceding density converges to the Gaussian density

$$p_{\eta_1} = \exp(-\eta_1^2 / 2) / \sqrt{2\pi} ; \quad |\eta_1| < \infty, \quad (19)$$

appropriate to η_1 .

Scaled linear ξ is Rayleigh-distributed, with the probability density and exceedance distribution described, respectively, by

$$p_\xi = \xi \exp(-\xi^2 / 2), \quad (20)$$

$$Q_\xi = \exp(-\xi^2 / 2). \quad (21)$$

Assuming narrowband waves, the probability density and exceedance distribution of scaled wave heights $h \approx 2\xi$ are given, respectively, by

$$p_{2\xi}(h) = (h/4) \exp(-h^2 / 4), \quad (22)$$

$$Q_{2\xi}(h) = \exp(-h^2/8). \quad (23)$$

These are variants of the Rayleigh law and valid as $\nu \rightarrow 0$. However, wind seas are not narrowband, and $h < 2\xi$ always. As a result, (23) overestimates the actual heights of large waves by as much as 8-10% [21]. Alternatively, large wave heights can be described more accurately by asymptotic models [15]-[18], [18]. For example, the Boccotti asymptotic model [18] leads to the probability density and exceedance distribution

$$p_h = 2c_0c_1 h \exp(-c_1 h^2), \quad (24)$$

$$Q_h = c_0 \exp(-c_1 h^2), \quad (25)$$

where $h \gg 1$, and $c_0 \geq 1$ and $c_1 \leq 1/4$ are coefficients dependent on two specific parameters inferred from the autocorrelation of surface elevations. They are elaborated elsewhere [15]-[18] and not repeated here. In general, second-order corrections do not affect (24) and (25) [15]-[22].

Second-order scaled crest ξ^+ and trough ξ^- amplitudes associated with large waves are asymptotically described by the quadratic expressions [20]

$$\xi^\pm = \xi \pm (1/2)\mu\xi^2, \quad (26)$$

where $\xi \gg 1$. Clearly, ξ^+ and ξ^- are mirror images or simply symmetric with respect to the Rayleigh-distributed linear ξ . A change of variables in (20) via (26) yields the probability densities [20], [21]

$$p_{\xi^\pm}(\xi^\pm) = \exp(-\xi^2/2) / |1 \pm \mu\xi|. \quad (27)$$

C. Comparisons with Oceanic Data

To compare the preceding theoretical results to actual statistics observed under oceanic conditions, we consider 9-hour measurements gathered with a Marex radar from the Tern platform in 167 m water depth in the northern North Sea during a severe storm in January, 1993 [10], [20]. This data set, hereafter simply referred to as Tern, represents severe stormy seas with wave heights as large as 25 m and crest exceeding 15 m. The sampling rate of surface time series is 5.12 Hz. The analysis of hourly segments gives $\sigma = 3.02$ m, spectral-peak period $T_p \approx 14.1$ s, $\lambda_3 = 0.172$, $\mu \approx 0.06$, $\varepsilon_p = 0.061$ and $\nu = 0.63$ as overall averages, and a total of 3,164 zero up-crossing waves. All the preceding parameters somewhat vary over time. For instance, the hourly σ estimates vary so that $2.85 \text{ m} \leq \sigma \leq 3.25 \text{ m}$. To compensate for this variability, all statistics estimated from hourly surface series were scaled with the corresponding segmental σ estimates.

Fig. 3 shows an overall average of hourly frequency spectra in a dimensionless form $S^* = \omega_p S(\omega)/m_0$ versus $u = \omega/\omega_p$, where ω_p = spectral-peak frequency. The product $u^4 S^*$ plotted in the same figure suggests that S has a high-frequency slope proportional to ω^{-4} approximately.

By setting $a \approx \sigma h/2$, (4) is rewritten as

$$h \leq 0.896 \tanh q / \sigma k = h_{\max}. \quad (28)$$

Fig. 4 shows a comparison of the upper bound of the preceding expression, h_{\max} , with the scatter of observed wave heights h and zero up-crossing periods T scaled with the spectral mean period $T_m = 2\pi m_0/m_1 = 11.2$ s. Clearly, larger wave heights lie below h_{\max} . Further, a short section of the surface profile around the deepest wave trough observed and shown in Fig. 5 displays no anomalous troughs with spurious secondary crests, if one allows for instrumental noise and inaccuracies due to oceanic spray and digital sampling.

Fig. 6 (a) compares the surface-elevation densities observed to the theoretical expressions (18) and (19). Similarly, Fig. 6 (b) contrasts the densities of crest and trough amplitudes observed to the Rayleigh and second-order densities described by (20) and (27), respectively. Finally, Fig. 6 (c) shows the variation of the ratio h/h_R with Q_h , where h stands for the observed or theoretical wave height predicted from (25), and $h_R = 2[-2 \ln(Q_h)]^{1/2}$ denotes the Rayleigh-distributed wave height inferred from (23) by setting $Q_{2\xi} = Q_h$. It appears that for larger waves, the general agreement between the data and model predictions are quite favorable in all cases. Though not shown here, the statistics of other surface features observed in Tern such as wave envelopes and wave phases also compare quite well with the second-order theoretical results [4], [11], [13].

III. EFFECTS OF SPURIOUS CRESTS

A. Threshold for Spurious-Crest Occurrences

The apparent inference that one can draw from the preceding comparisons and many others elsewhere, e. g. [4]-[5], [8]-[14], is that the standard model works generally works

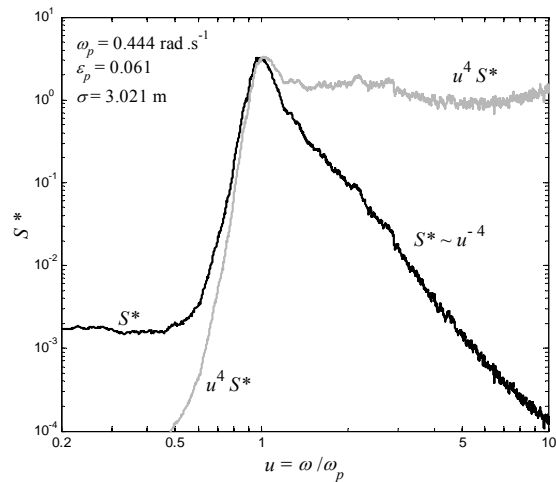


Fig. 3 Tern: frequency spectrum $S^* = \omega_p S / m_0$ versus ω / ω_p

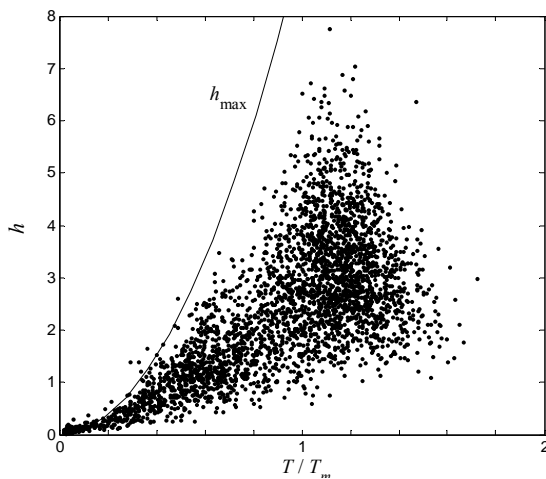


Fig. 4 Tern: scatter diagram of wave heights and periods

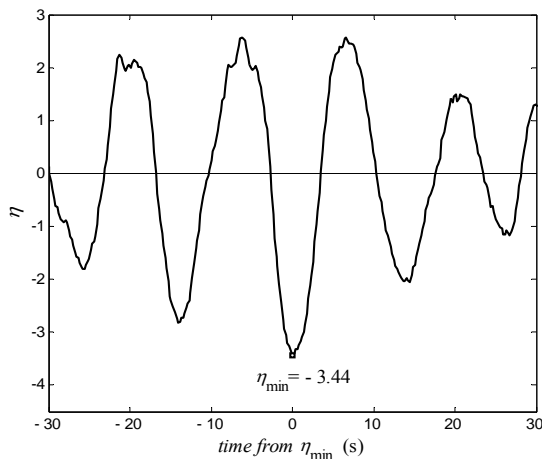


Fig. 5 Tern: surface profile around the deepest wave trough

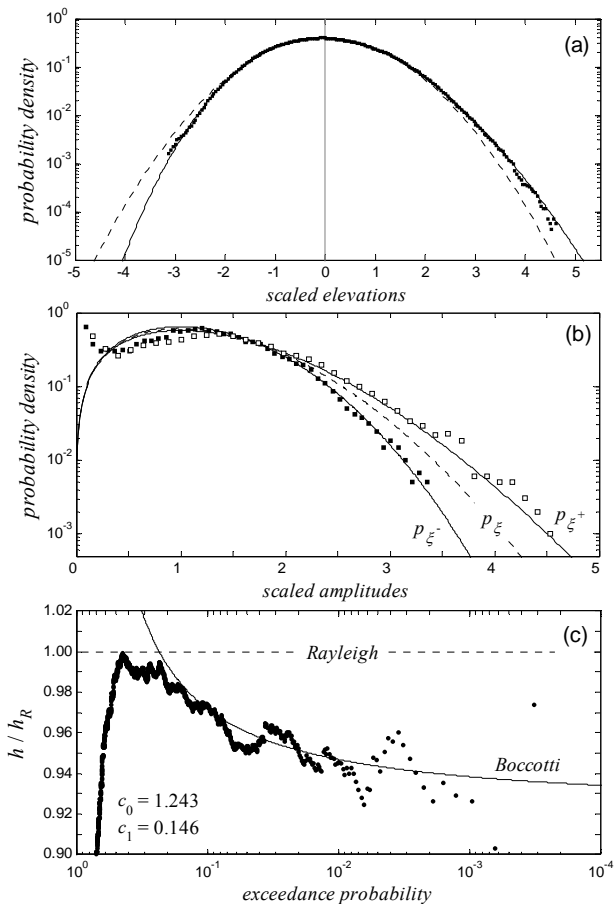


Fig. 6 Tern data (discrete) vs. linear (dashed) and second-order predictions (continuous): (a) surface elevations compared to second-order (18) and linear Gaussian (19) densities; (b) crest and trough amplitudes vs. Rayleigh (20) and second-order (27) predictions; and, (c) wave heights vs. Rayleigh (23) and Boccotti (25) distributions

quite well in describing the statistics of various surface features in simple wind seas. However, most of these comparisons rely on statistics estimated from sample populations of limited size, similar to the present comparisons with the Tern data. Large populations of measurements representative of relatively extreme and homogeneous wind seas are scarce. Inhomogeneous trends often observed in the spectral and statistical characteristics of oceanic storm seas lead to additional complications. In particular, the presence of third- and higher-order nonlinear interactions in such seas can cause the observed statistics to deviate significantly from the second-order predictions.

Even under idealized conditions of statistical homogeneity, and in the absence of third- and higher-order nonlinear effects and surface stresses, the probability structure of various surface features is either unknown at all or can only be described approximately or asymptotically. A similar inference is also valid for the kinematics and dynamics of the wave-induced fluid motions. Of course, the nature of all these can be explored via simulations of large sample populations from the standard model, e.g. as in [20]–[21], for wave heights

and crests. Intuitively, the larger a simulated sample population becomes, the more likely it is to include intermittent occurrences of relatively rare, large surface displacements arising from the constructive interference of a sufficiently large number of spectral components of different frequencies and amplitudes, thus leading to wave forms with large crest and/or trough amplitudes. The question is then if all of these would be representative of realistic waves within the range of relative validity of the second-order model devoid of anomalous troughs. As will be shown in the following, the answer is not always affirmative.

A probabilistic analysis of spurious crests on relatively deep wave troughs requires the joint probability density of η and its first two time derivatives. The exact form of that density is not known, and possible approximations to it, e.g., by way of Gram-Charlier series expansions lead to functional forms that violate the non-negativity condition for large negative values of η , as is well known. An alternative approach is to draw upon the expected structure of the second-order surface around a deep trough. Given the spectrum, this approach makes it possible in an average sense to determine a threshold for trough amplitudes beyond which spurious-crest occurrences are more likely.

Assume for the moment that we observe a relatively large negative minimum $\eta_1(t_o)$ of η_1 at $t = t_o$. Since the scaled linear surface has the equivalent form $\eta_1 = \xi(t) \cos \phi(t)$, where $\tan \phi = \dot{\eta}_1 / \eta_1$, it is easily verified that

$$\eta_1(t_o) = -\xi / [1 + (\dot{\xi} / \xi \dot{\phi})^2]^{1/2} \Big|_{t=t_o}. \quad (29)$$

Given ξ , the joint probability structure of $\dot{\xi}$ and $\dot{\phi}$ [28] indicates that $\dot{\xi}$ is independent of ξ and Gaussian with zero-mean and standard deviation $\omega_m v$, and that $\dot{\phi}$ is also Gaussian but with mean ω_m and standard deviation $\omega_m v / \xi$. So, $\dot{\xi} = O(\omega_m v)$ and $\dot{\phi} / \omega_m = 1 \pm O(v / \xi)$. These results allow one to rewrite (29) as

$$\eta_1(t_o) = -\xi [1 - O(v / \xi)^2 + \dots]. \quad (30)$$

Therefore, $\eta_1(t_o) = -\xi$ with an error of at most $O(v / \xi)^2$ that diminishes for sufficiently large ξ since $v < 1$ in simple wind seas.

The expected profile of $\eta_1(t_o + \tau)$, given $A \equiv \{ \eta_1(t_o) < -\xi \ll -1 \}$, follows in present notation from [24] as

$$\bar{\eta}_1 = \langle \eta_1(t_o + \tau) | A \rangle = -C_\xi \rho(\tau), \quad (31)$$

with $\rho(\tau) = \langle \eta_1(t_o) \eta_1(t_o + \tau) \rangle \equiv$ autocorrelation function, and

$$C_\xi = \langle \eta_1(t_o) | A \rangle = \sqrt{\frac{2}{\pi}} \frac{\exp(-\xi^2/2)}{\operatorname{erfc}(\xi/\sqrt{2})}. \quad (32)$$

For $\xi \gg 1$, $C_\xi = \xi / [1 - \xi^{-2} + 3\xi^{-4} - \dots]$ so that $C_\xi \rightarrow \xi$ as $\xi \rightarrow \infty$. Now, note that replacing C_ξ with ξ coupled with a sign change in (31) yields the expected surface profile around an exceptionally large crest, as in [17] and [23].

The expected profile of $\eta(t_o + \tau)$, given A , is easily obtained from (31) as [29],

$$\bar{\eta} = \langle \eta(t_o + \tau) | A \rangle = C_\xi [-\rho(\tau) + (C_\xi/6) \lambda(\tau)], \quad (33)$$

where

$$\lambda(\tau) = \frac{3}{2m_0^{3/2}} \iint (H^+ + H^-) E(\mathbf{k}) E(\mathbf{k}') d\mathbf{k} d\mathbf{k}', \quad (34)$$

with

$$H^\pm = K^\pm \cos(\omega \pm \omega') \tau. \quad (35)$$

Again, considering the limit case $C_\xi \rightarrow \xi$ as $\xi \rightarrow \infty$ and changing the sign of ρ in (33) will lead to the expected surface profile around an exceptionally large crest, as in [14]-[15] and [18]-[22].

The occurrence of spurious crests at wave troughs requires that the second derivative of $\bar{\eta}$ at $\tau = 0$ be negative. Explicitly,

$$C_\xi [-\ddot{\rho}(0) + C_\xi \ddot{\lambda}(0)/6] \leq 0, \quad (36)$$

where

$$\ddot{\rho}(0) = -m_2 / m_0, \quad (37)$$

$$\ddot{\lambda}(0) = -3(I^+ + I^-) / 2m_0^{3/2}, \quad (38)$$

$$I^\pm = \iint (\omega \pm \omega')^2 K^\pm E(\mathbf{k}) E(\mathbf{k}') d\mathbf{k} d\mathbf{k}'. \quad (39)$$

The solution, say, ξ^* of the upper limit of (36), namely

$$C_{\xi^*} = 4m_0^{1/2} m_2 / (I^+ + I^-) \quad (40)$$

provides the threshold beyond which wave troughs exhibit spurious crests. Numerically, ξ^* follows with ease from a few iterations of the Newton-Raphson scheme, taking the right-hand-side of (40) as an initial estimate for ξ^* .

For long-crested waves travelling all in the same direction in deep water, $K^\pm = \pm |\omega^2 \pm \omega'^2| / g$. On this basis, one can show that $I^+ = 2(m_2^2 + 2m_1 m_3 + m_0 m_4) / g > 0$, $I^- \leq 0$, and $I^+ \gg |I^-|$. If ξ is also sufficiently large so that $C_\xi \approx \xi$, then (40) can be approximated as

$$\xi^* \approx 2g m_0^{1/2} m_2 / (m_2^2 + 2m_1 m_3 + m_0 m_4). \quad (41)$$

For long-crested narrowband waves in deep water, the

second-order model reduces to [12], [21]

$$\eta = \eta_1 + \eta_2 = \xi \cos \phi + \frac{1}{2} \mu \xi^2 \cos 2\phi, \quad (42)$$

where $\mu \approx m_0^{1/2} \omega_m^2 / g \approx \lambda_3 / 3$, and $\phi(t)$ is the phase function, independent of ξ and uniformly distributed over an interval of 2π such that $\langle \dot{\phi} \rangle = \omega_m$. It can be verified that given ξ , (42) exhibits spurious crests if $\xi > \xi^* = 1/2\mu$. Thus, (42) is valid for $\eta > -1/2\mu$, consistent with the domain of p_η in (18).

Consider now the narrowband limit of (40). If $\xi \gg 1$ as $v \rightarrow 0$, $m_j \rightarrow m_0 \omega_m^j$, $I^+ = 8m_0^2 \omega_m^4$ and $I^- = 0$ identically, thus reducing (40) to the threshold

$$C_{\xi^*} \approx \xi^* = 1/2\mu, \quad (43)$$

consistent with the narrowband approximation (42).

When ξ^* is sufficiently large, the exceedance frequency of waves with anomalous troughs follows from (21) as

$$Q_{\xi^*} \approx Q_{\xi}(\xi^*) = \exp(-\xi^{*2} / 2). \quad (44)$$

This expression provides an estimate for the fraction of zero up- or down-crossing waves likely to be affected by anomalous troughs with spurious crests.

B. Numerical Results and Simulations

Consider directional frequency spectra described by

$$F(\omega, \theta) = \alpha S^*(u) D(\theta), \quad (45)$$

$$S^*(u) = (m_0 / \omega_p) u^{-n} \exp(-a u^{-4}) \gamma^{g(u)}, \quad (46)$$

$$D(\theta) = \beta^{-1} \cos^2(\pi \theta / 2\beta), \quad (47)$$

where $u = \omega / \omega_p > 0$, $|\theta| < \beta \leq \pi/2$. For $n = 5$ and $a = 5/4$, S^* represents the non-dimensional form of the conventional JONSWAP spectrum. Setting $n = 4$ and $a = 1$, as in [30], modifies (46) so as to mimic spectra that tend to u^{-4} for $u \gg 1$ as opposed to the u^{-5} tail of the conventional formulation. In either case, γ = peak-enhancement coefficient, $g(u)$ = standard JONSWAP exponent function, and α = dimensionless constant such that the volume under F equals m_0 . For the average JONSWAP spectrum $\gamma = 3.3$. The frequency spectra estimated from hourly segments of Tern are described well by (46) with $\gamma \approx 2.5\text{--}3.5$ for $2 < u < 10$, approximately.

In implementing the conventional or modified JONSWAP spectrum in linear Gaussian simulations, it is necessary to band-limit the spectral domain to an upper frequency cut-off to avoid unstable fourth- and higher-order moments. This not only raises awkward questions as to what the cut-off frequency should be, but also it presents a further point of concern in second-order simulations, particularly if η_1 is described by a spectrum that tends to ω^{-n} over high

frequencies. Second-order corrections on linear spectra are $O(\omega^4)$ and non-negative. They tend to amplify linear spectral amplitudes on either side of the spectral peak, mostly away from it. The resulting second-order η is then characterized by a spectrum that tends to ω^{-n+4} . So, it is obvious that if the linear spectrum is similar to a conventional or modified JONSWAP form and defined over an unbounded frequency range, it needs to be tapered to attenuate as ω^{-8} or ω^{-9} , respectively, starting at some frequency sufficiently greater than the spectral-peak frequency ω_p . So, in simulating second-order surface series from a linear conventional or modified form of (46), we will band-pass (46) so that $0.2 < u < 10$ and also taper it by $w(u) = (3.5/u)^4$ for $u > 3.5$. Band-passing and tapering (46) in the manner described leads to simulated non-linear spectra effectively similar to the non-tapered form of (46) used in linear simulations for $0.2 < u < 10$. Numerical computations on the tapered form of the modified JONSWAP spectrum indicate that in reducing the upper cut-off from $u = 30$ to 10 , spectral moments m_j for $j = 0, 1, \dots, 4$ do not vary significantly. The most noticeable variation is seen in m_4 as reduction of about 1.3%.

The frequency-independent nature of the directional distribution (47) is not altogether realistic, but it is merely of convenience for the numerical computations of ξ^* from (40). The parameter β in radians controls the directional bandwidth. As $\beta \rightarrow 0$, waves become long-crested and travel all in the same direction while as $\beta \rightarrow \pi/2$, they become short-crested. Fig. 8 illustrates directional distributions described by (47) for $\beta = 0, \pi/12, \pi/8, \dots, \pi/2$, all indicated in degrees in the figure.

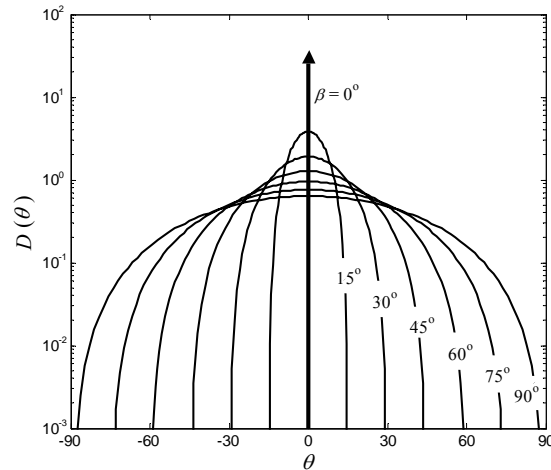


Fig. 7 Directional distribution (47) for various β

Consider now waves described by (45)-(47) at deep water, and assume that $\sigma = 3$ m, $T_p = 14$ s and $\varepsilon_p = 0.061$, similar to Tern. The numerical solutions for ξ^* would then follow via four-fold numerical integration from (39)-(40) based on the tapered and band-limited forms of the conventional and modified JONSWAP formulations. The results for various values of angular spread β are summarized in Table I. Repeating the same exercise at shallower water depths of $d =$

100 m ($q \geq \pi/11$ and $q_p = k_p d = 2.11$) and $d = 50$ m ($q \geq \pi/16$ and $q_p = 1.2$) leads to the results in Tables II and III, respectively. In all three tables, the fraction Q_{ζ^*} of waves whose trough amplitudes exceed ζ^* is displayed as $10^5 Q_{\zeta^*}$, approximating the number of spurious crests that one can on average expect in a sample population of 10^5 waves. A quick review of the values in Tables I-III indicates that spurious occurrences are most pronounced in long-crested waves described by spectra similar to the modified JONSWAP form that tends to ω^{-4} . While such occurrences tend to decrease and become less significant as the angular spread of waves widens, they increase dramatically at shallower depths. What all this means is that given $\zeta^* \gg 1$, one can expect the simulated statistics of second-order elevations η , trough amplitudes ζ^- , and thus exceedance frequency distribution of wave heights Q_h to progressively deviate from the theoretical predictions for

60°	3.2326	538.1	2.717	2492
75°	3.5822	163.5	3.026	1026
90°	4.0081	32.47	3.407	301.8

$$\eta < -\zeta^*[1 - (1/2)\mu\zeta^*], \quad (48)$$

$$\zeta^- > \zeta^*[1 - (1/2)\mu\zeta^*], \quad (49)$$

and $Q_h < Q^*$.

The preceding expressions are approximations inferred from the expected shape of the surface around a sufficiently deep trough. They indicate what we can expect to see in an average sense. In actual realizations, negative surface elevations and wave troughs that satisfy the constraints (48) and (49) may not all exhibit spurious crests. Conversely, some negative surface elevations and wave troughs that do not satisfy (48) and (49) may also exhibit spurious crests, albeit less likely than when (48) and (49) are satisfied.

The simulation of a sufficiently large sample population of directional waves in deep or shallow water requires a rather cumbersome computational effort, demanding a good deal of memory. This may not be necessary for illustrating the general nature of the principal results developed here. As a simpler alternative, consider two simple cases, A and B, for simulating long-crested deep-water waves described by a modified JONSWAP spectrum. Table IV shows the target values of σ and T_p selected in each case for simulating non-tapered linear, tapered linear and second-order surface series to be generated from the latter. Clearly, linear and non-linear waves in case A have similar characteristics to those observed in Tern whereas case B represents relatively less steep or gentler waves. In both cases, the simulations are easily carried out to generate fairly large populations of more than 10^5 waves, using 20 iterations of an efficient procedure elaborated in [22]. The same table also summarizes the number of waves, and the principal spectral and statistical parameters simulated. The simulated values of σ and T_p are effectively the same as the target values.

In each case, we first simulate linear waves from the non-tapered spectrum, identified with the heading “linear” in Table IV. A particular result such as a scatter diagram, a probability density or distribution estimated from these serves as a relative reference for comparing a corresponding non-linear result. In order to make the eventual comparisons between the linear and non-linear waves compatible, it is necessary to use the same sets of random phases, i. e. ε in (8), for both non-tapered and tapered linear simulations before one proceeds to generate second-order corrections (14) from the tapered linear simulations. Linear series simulated from the tapered spectrum are tagged as “tapered”, and second-order series that follow from these are simply denoted as “non-linear” in the table. Finally, note that second-order corrections always tend to increase m_0 and thus σ slightly. So, a tapered linear series needs to be simulated with a slightly smaller value of σ than that of the non-tapered linear series to obtain a second-order series characterized by a σ value that is nearly the same as that

TABLE I
THRESHOLDS FOR SPURIOUS CRESTS IN DEEP WATER

β	JONSWAP $\sim \omega^{-5}$		modified JONSWAP $\sim \omega^{-4}$	
	ζ^*	$10^5 Q^*$	ζ^*	$10^5 Q^*$
0°	4.062	26.13	3.103	810.2
15°	4.118	20.79	3.148	706.0
30°	4.287	10.22	3.281	459.6
45°	4.572	2.890	3.506	214.0
60°	4.978	0.415	3.827	65.94
75°	5.513	0.025	4.250	11.95
90°	6.185	0.000	4.783	1.075

TABLE II
THRESHOLDS FOR SPURIOUS CRESTS IN TRANSITIONAL WATER: $d = 100$ m

β	JONSWAP $\sim \omega^{-5}$		modified JONSWAP $\sim \omega^{-4}$	
	ζ^*	$10^5 Q^*$	ζ^*	$10^5 Q^*$
0°	3.800	73.17	2.940	1327
15°	3.852	59.90	2.9822	1172
30°	4.011	32.07	3.1098	794.2
45°	4.279	10.57	3.3249	397.6
60°	4.660	1.930	3.6308	137.2
75°	5.158	0.167	4.0326	29.43
90°	5.782	0.006	4.5373	3.384

TABLE III
THRESHOLDS FOR SPURIOUS CREST IN TRANSITIONAL WATER: $d = 50$ m

β	JONSWAP $\sim \omega^{-5}$		modified JONSWAP $\sim \omega^{-4}$	
	ζ^*	$10^5 Q^*$	ζ^*	$10^5 Q^*$
0°	2.6105	3313	2.173	9441
15°	2.6487	2996	2.206	8775
30°	2.7653	2185	2.308	6975
45°	2.9601	1251	2.478	4640

of the non-tapered linear series. Otherwise, the eventual comparisons between the non-tapered linear and non-linear series generated from the tapered linear series would be distorted as a result of scaling each with a different σ .

C. Comparisons

Fig. 8 shows the scatter diagrams of wave heights and periods simulated in comparison with the upper bound described by $H_{\max} = 0.0227gT^2$, which follows from (4) or (28) in deep water. In Fig. 8 (a) and (b) appropriate respectively to the linear and non-linear waves simulated in case A, some wave heights appear to exceed H_{\max} . However, nearly all waves with heights larger than 4σ do not. So, the statistics describing the heights, and crest and trough amplitudes of relatively large waves simulated in case A are not affected by the upper-bound limits implied by constraints such as (4) or its refinements [6]. Evidently, the

same conclusion is also valid nearly for all waves of case B, shown in Fig 8 (c) and (d).

Fig. 9 compares the densities of simulated surface displacements to (18) and (19). The thresholds below which η should be affected by spurious crests are from (48) or Table IV and included in the figure. For case A in Fig. 10 (a), where about 0.81% of wave troughs or about 880 out of 108,464 non-linear waves simulated are expected to display spurious crests, the comparisons tend to confirm the validity of the expected threshold -2.78 quite well as the observed density of non-linear η progressively exceeds the theoretical density (18) when $\eta < -2.78$, approximately. This does not happen in case B where the threshold is noticeably lower and nearly coincident with the lower limit of negative values of simulated surface series. In order to observe possible effects of spurious crests in this case, it would be necessary to simulate much longer surface series and thus many more waves than simulated here.

The comparisons of densities describing simulated crest and trough amplitudes to the corresponding theoretical predictions from (27) are shown in Fig. 10 (a) and (b) for cases A and B, respectively. The same figures also include, from (49) or Table IV, the thresholds above which simulated trough amplitudes can be expected to display spurious effects. The distortions and/or amplifications of the density of simulated trough amplitudes are seen in Fig. 10 (a) for case A, but they are manifest more clearly at amplitudes somewhat larger than the theoretically expected threshold of 2.78. Otherwise, the overall nature of results displayed here is similar to Fig. 9 (a) and (b).

Finally, the comparisons between the simulated h/h_R ratios and the corresponding theoretical predictions from (23) are shown in Fig. 11 (a) and (b). Notice that the thresholds, namely Q^* estimates appropriate to both cases are given in Table IV. These are included in Fig. 11. In particular, Fig. 11 (a) clearly shows that for $Q_h < Q^*$, spurious occurrences amplify the heights of non-linear waves simulated in case A, and cause them to appear progressively larger than they should be within the realistic range of the second-order theory. Similar effects do not appear in case B of Fig. 11 (b) since $Q^* \approx 1.14 \times 10^{-5}$, suggesting that less than 0.00114% of all simulated non-linear waves or 1-2 out of 119,717 waves are likely to be affected by spurious crests.

IV. CONCLUSIONS

Occurrences of anomalous wave troughs characterized by spurious crests are not a typical feature of wind waves. However, they arise as a systemic source of error in the statistics describing large negative surface displacements, trough amplitudes and thus the heights of relatively large and steep waves simulated via the standard second-order model. Spurious occurrences do not affect wave crests.

The threshold criterion developed here appears to be reasonably effective in exploring how and to what extent spurious crests affect the statistics derived from a large population of waves simulated via the standard second-order model. Numerical results from idealized forms of directional

	case A			case B		
	linear	tapered	non-linear	linear	tapered	non-linear
waves	109,563	107,387	108,464	127,706	119,444	119,717
σ (m)	3.00	2.95	3.00	1.50	1.49	1.50
T_p (s)	14	14	14	12	12	12
T_m (s)	10.74	11.07	8.12	9.21	9.49	7.62
ν	0.51	0.41	0.54	0.51	0.41	0.50
λ_3	0.00	0.00	0.204	0.00	0.00	0.140
μ	0.00	0.00	0.068	0.00	0.00	0.047
ε_p	0.062	0.061	0.061	0.042	0.042	0.042
ζ^*	∞	∞	3.10	∞	∞	4.77
$10^5 Q^*$	∞	∞	810	∞	∞	1.14

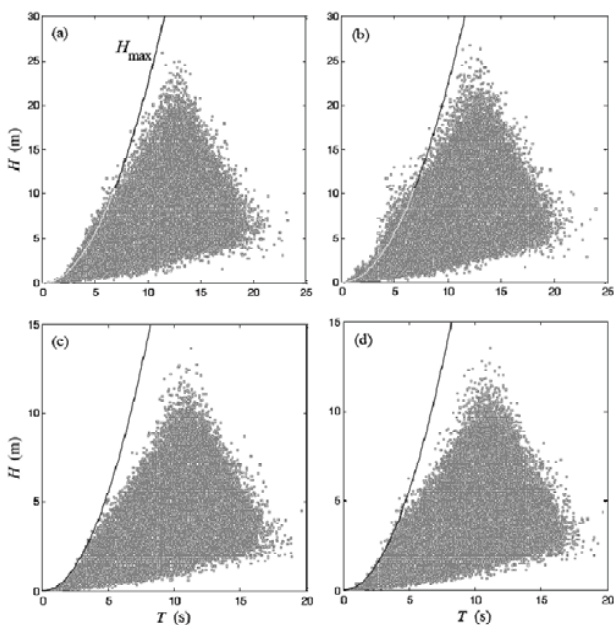


Fig. 8 Scatter of wave heights and periods observed in simulations compared to: (a) case A linear waves, (b) case A non-linear waves, (c) case B linear waves, and (d) case B non-linear waves

surface spectra, albeit limited, indicate that effects of spurious occurrences are most pronounced in simulations mimicking long-crested seas, especially at relatively shallower water depths. As to be expected, this is consistent with the general nature of deterministic second-order Stokes theory. Effects of spurious occurrences tend to diminish with the angular spread of simulated waves, in particular, at deep water.

Several theoretical expressions considered here and developed from the standard second-order model appear to be quite effective in describing the statistics of various surface features in large oceanic waves. Significant discrepancies between these expressions and oceanic data do not arise often. This is mainly because most comparisons typically rely on sample populations of limited size or use a large composite of small populations from different sea states. Theoretical expressions derived from the standard second-order stochastic theory are valid over a restricted domain closely associated with the occurrence of spurious crests. Thus, significant errors or discrepancies may not appear between the second-order predictions and actual data unless measurements represent shallow-water waves, or they are sufficiently extensive, comprising large negative surface displacements outside the domain of validity of theoretical expressions.

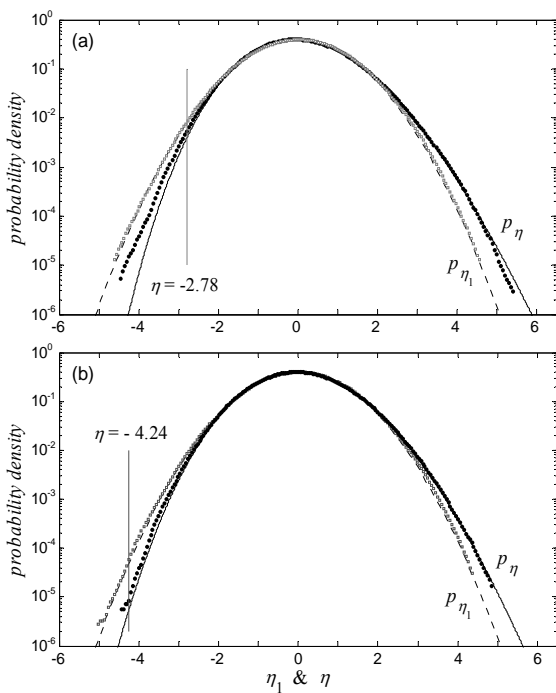


Fig. 9 Probability densities of simulated linear and non-linear surface elevations in comparisons with theoretical densities (18) and (19): (a) case A, and (b) case B

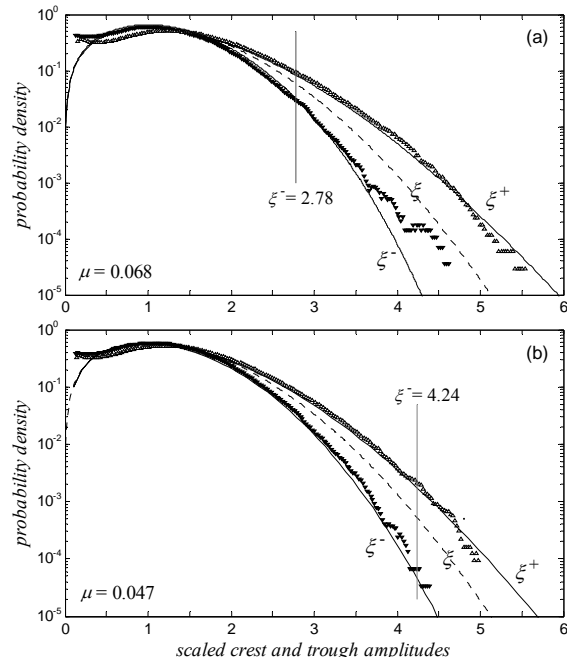


Fig. 10 Probability densities of simulated non-linear crest and trough amplitudes in comparisons with predictions from (27): (a) case A, and (b) case B

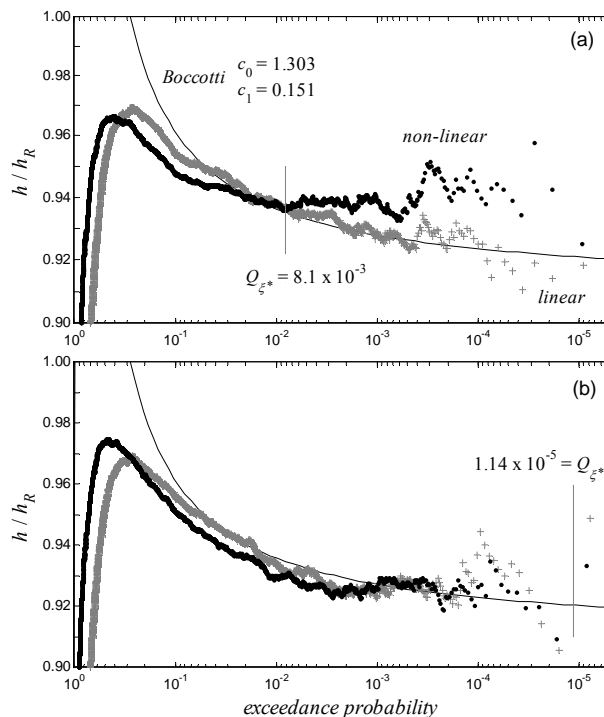


Fig. 11 Wave-height ratios h/h_R simulated (discrete) in comparisons with theoretical ratios (continuous) from Boccotti distribution (25): (a) case A, and (b) case B

REFERENCES

- [1] R. G. Dean, and R. A. Dalrymple, *Water Wave Mechanics for Engineers and Scientist.*, New Jersey: World Scientific, 1991, pp. 295-305.
- [2] R. Miche, "Mouvements ondulatoires de la mer en profondeur onstante ou decroissante. Annales des Ponts et Chaussees," vol. 121, pp. 285-318, 1944.
- [3] M. P. Tulin, and J. J. Li, "On the breaking of energetic waves," *Inter. J. Offshore Polar Eng.*, vol. 2, pp. 46-53, 1992.
- [4] M. A. Tayfun, "Distributions of envelope and phase in wind waves," *J. Phys. Oceanogr.*, vol. 38, pp. 2784-2800, 2008.
- [5] Z. Cherneva, M. A. Tayfun, and C. Guedes Soares, 2009. "Statistics of nonlinear waves generated in an offshore wave basin," *J. Geophys. Res.*, vol. 114, C08005, doi:10.1029/2009JC005332, 2009.
- [6] A. Toffoli, A. Babanin, M. Onorato, and T. Waseda, "Maximum steepness of oceanic waves: field and laboratory experiments," *Geophys. Res. Lett.*, vol. 37, L05603, doi:10.1029/2009GL041771, 2010.
- [7] J. N. Sharma, and R. G. Dean, "Development and evaluation of a procedure for simulating a random directional second order sea surface and associated wave forces," *Ocean Eng. Rep.* 20, University of Delaware, Newark. 1979.
- [8] M. S. Longuet-Higgins, "The effects of nonlinearities on statistical distributions in the theory of sea waves," *J. Fluid Mech.* vol. 17, pp. 459-480, 1963.
- [9] L. Weber, and D. E. Barrick, "On the nonlinear theory for gravity waves on the ocean's surface. Part I: derivations," *J. Phys. Oceanogr.*, vol. 7, pp. 3-10, 1977.
- [10] G. Z. Forristall, "Wave crest distributions: observations and second-order theory," *J. Phys. Oceanogr.*, vol. 30, pp. 1931-1943, 2000.
- [11] M. A. Tayfun, "Distributions of envelope and phase in weakly nonlinear Random waves," *J. Eng. Mech.*, vol. 120, pp. 1009-1025, 1994.
- [12] M. A. Tayfun, "Narrow-band nonlinear sea waves," *J. Geophys. Res.*, vol. 85, pp. 1548-1552, 1980.
- [13] M. A. Tayfun, and J-M. Lo, "Envelope, phase, and narrowband models of sea waves," *J. Waterw. Port. Coast. Ocean Eng.*, vol. 115, pp. 594-613, 1990.
- [14] F. Arena, and F. Fedele, "A family of narrow-band nonlinear stochastic processes for the mechanics of sea waves," *Eur. J. Mech. B/Fluids*, vol. 21, pp. 125-137, 2005.
- [15] M. A. Tayfun, "Distribution of large wave heights," *J. Waterway, Port, Coast. Ocean Eng.*, vol. 116, pp. 686-707, 1990.
- [16] P. Boccotti, "On mechanics of irregular gravity waves," *Atti Acc. Naz. Lincei Memorie*, vol. 19, pp. 111-170, 1989.
- [17] P. Boccotti, *Wave mechanics for ocean engineering*, Oxford: Elsevier Science, 2000, pp. 475-485.
- [18] F. Arena, "On non-linear very large sea wave groups," *Ocean Eng.*, vol. 32, pp. 1311-1331, 2005.
- [19] F. Fedele, and F. Arena, "Weakly nonlinear statistics of high random waves," *Phys. Fluids*, vol. 17, pp. 026601:1-10, 2005.
- [20] F. Fedele, and M. A. Tayfun, "On nonlinear wave groups and crest statistics," *J. Fluid Mech.*, vol. 620, pp. 221-239, 2009.
- [21] M. A. Tayfun, and F. Fedele, "Wave-height distributions and nonlinear effects," *Ocean Eng.*, vol. 34, pp. 1631-1649, 2007.
- [22] M. A. Tayfun, "On the distribution of wave heights: nonlinear effects," in *Marine Technology and Engineering*, vol. 1, C. Guedes Soares, Y. Garbatov, N. Fonseca, and A. P. Teixeira, Eds. London: Taylor & Francis Group, 2011, pp. 247-268.
- [23] G. Lindgren, "Local maxima of Gaussian fields," *Arkiv för Matematik*, vol. 10, pp. 195-218, 1972.
- [24] O. M. Phillips, D. Gu, and M. Donelan, "On the expected structure of extreme waves in a Gaussian sea. I. Theory and SWADE buoy measurements," *J. Phys. Oceanogr.*, vol. 23, pp. 992-1000, 1993.
- [25] A. Toffoli, E. Bitner-Gregersen, M. Onorato, A. R. Osborne, and A. V. Babanin, "Surface gravity waves from direct numerical simulations of the Euler equations: A comparison with second-order theory," *Ocean Eng.*, vol. 35, pp. 367-379, 2008.
- [26] M. A. Tayfun, "Statistics of nonlinear wave crests and groups," *Ocean Eng.*, vol. 33, pp. 1589-1622, 2006.
- [27] M. A. Tayfun, "A modified probability distribution for describing second-order sea waves," unpublished.
- [28] M. S. Longuet-Higgins, *The statistical analysis of a random moving surface*. Philos. Trans. Roy. Soc. London, A966, pp. 321-387, 1957.
- [29] M. A. Tayfun, and F. Fedele, "Expected shape of extreme waves in storm seas," in *Proc. 26th Inter. Conf. on Offshore Mech. & Arctic Eng.*, San Diego, paper no. OMAE2007-29073, pp. 1-8, 2007.
- [30] M. A. Donelan, J. Hamilton, and W. H. Hue, "Directional spectra of wind-generated waves," *Philos. Trans. Roy. Soc. London*, A315, pp. 509-562, 1985.